IPNO-DRE-94-23

Stripping properties of a plasma medium for MeV/u chlorine Ions

M.Chabot, D.Gardès, P.Box, J.Kiener,
C.Deutsch, G.Maynard, V.André,
C.Fleurier, D.Hong, K.Wohrer

Stripping properties of a plasma medium for MeV/u chlorine Ions

M.Chabot, D.Gardès, P.Box, J.Kiener[1], C.Deutsch, G.Maynard[2], V.André, C.Fleurier, D.Hong[3] , K.Wohrer[4]

[1] *Institut de Physique Nucléaire, Orsay (IN2P3) - GDR 918*

[2] *Laboratoire de Physique des Gaz et des Plasmas, Orsay - GDR 918*

[3] *Groupe de Recherche sur l'Energétique et la Matière Ionisée, Orléans - GDR 918*

[4] *Groupe de Physique des Solides, ParisVII*

Abstract

A clear experimental evidence of plasma stripping enhancement for chlorine ions in the MeV/u energy range is contrasted to its cold gas homologue at same density. The velocity dependence for the charge distributions is modelized both in cold gas and in plasma experiments. Calculations are found to be in good agreement with the hypothesis of a strongly reduced capture in the plasma case.

1-Introduction

Stripping properties of solid and gaseous media have been extensively studied for many years, either for application in heavy-ion accelerators, or for basic physical issues.[1,2]. Implementation of plasma targets on accelerator beam-lines [3,4] opens the opportunity to investigate the stripping properties of this new medium.

When a swift heavy ion penetrates into a solid or gaseous medium it exchanges energy in collisions with bound electrons. During this process successive electron captures and losses occur leading to an equilibrium charge-state. In a plasma medium, electrons are free and the capture probability of free electrons depends on recombination processes associated with very low cross sections such as radiative transfer or dielectronic recombination [5,6]. As a result, an ion penetrating into a plasma should increase rapidly its charge state up to a value larger than the cold matter equilibrium charge.

This paper presents experimental evidence for such effects. The choice of the chlorine ion at 1.5 MeV/u was determined by the compromise between the ability to perform a complete theoretical treatment of the evolution of the charge-state distribution (high velocity and low atomic number) and, on the other hand, by the possibility for this particular collision, to produce a significant difference between the plasma and cold-gas target, which is expected to increase at low velocity and with high Z projectile.

In the first part, the experimental set-up is described and special attention is paid to the plasma characteristics. In a second part, a modelisation solving numerically a set of rate equations for the different final charge states, is compared to the experimental results for charge-state distributions in cold gas and plasma.

2- Experimental Set-up

Chlorine beams were delivered by the Orsay MP Tandem Van de Graaff accelerator. The negative ion source of the machine was run in a pulsed mode in order to access to high instantaneous intensities without destroying the stability of the voltage machine. The beam was transported through a 90° analyzing magnet and stripper device which allowed for the selection of a given charge state at the target entrance.

2-1 Cold gas target

A quartz tube (52 cm long and 0.5 cm diameter) was filled with hydrogen or deuterium gas, cycled with a continuous flow. The tube was enclosed between two fast valves [7] which were opened only during the measurement. The flow rate was regulated with a mass flow controller (accuracy $\pm$ 0.8%). The pressure was controlled with an absolute pressure gauge (baratron) with 0.5% accuracy. In these experiment the pressure ranged from 10^{-2} Torr up to 10 Torr. The beam arrival was synchronized with the tube unlocking. A laser beam transmission measurement showed that a time of 200 ± 5 µs was necessary for a full opening of the plasma tube by means of the fast valves. Therefore, the beam pulse was injected 200 µs after the start of the opening. During this short time the leakage flux through the collimators toward the beam line was measured and found to be 2.5 % of the starting pressure. Under secondary pumping, composition of the residual gas (2.10^{-3} torr) inside the tube was analysed by means of a mass spectrometer and found to arise mainly composed from water molecules.

2-2 Plasma Target

2-2-1 Design features

For the plasma target, the same quartz tube filled with hydrogen or deuterium, was fired using an electrical discharge through the gas. After a few μs the gas was completely ionized producing a plasma with a linear density of the order of 5.10^{19} e^-/cm^2. Under the influence of the discharge current and also because of gas ejection through the tube apertures, the electron density varied rapidly as a function of time. The complete exploration of the density range has been performed by synchronizing and varying the arrival time of a short ion-beam burst during the plasma evolution.

2-2-2 Plasma diagnostics

Density and temperature of the plasma were measured using methods already presented in ref.[8] which are based on: Stark line-broadening, laser absorption at two different wavelengths and laser interferometry. All diagnostic measurements were performed along the tube axis which is also the beam axis. Therefore, they could only be performed off-line without beam.

During on-line operations, the plasma was monitored by aid of transverse light emission. From this, stability and reproducibility of the plasma were derived. The density was obtained via thermodynamics and line-broadening models. This control is subject to larger uncertainty than in the longitudinal determination due to the small thickness of the plasma in this transverse direction and to a density gradient near the tubes wall.

Spectroscopic and optical methods are not very sensitive in detecting very small contamination rates of (heavy) impurities. However, such a contamination can strongly affect the evolution of the charge distribution of the chlorine ions relative to situations in pure plasma or cold-gas. For this purpose, an ion beam was used as a probe to investigate both heavy element impurities and proton density. The method is detailed in ref. [9] and [10]. The principle of the measurement is based on charge-exchange and ionization processes on an hydrogen-like chlorine ion beam (Cl^{16+}) at 4.3 MeV/u. For this particular beam, it is found that the main contributions for electron capture and ionization come from the heavy contaminants and the protons, respectively. In these conditions, measurements on Cl^{15+} helium-like ion production and Cl^{17+} bare ion-production provide respectively access to the heavy element and proton densities inside the plasma target. A good agreement was found with the optical diagnostic presented previously for the proton density and compatible with the residual pressure (2.10^{-3} torr) measurement for the heavy elements contamination. Fig.(1) presents the electron linear density as a function of time.

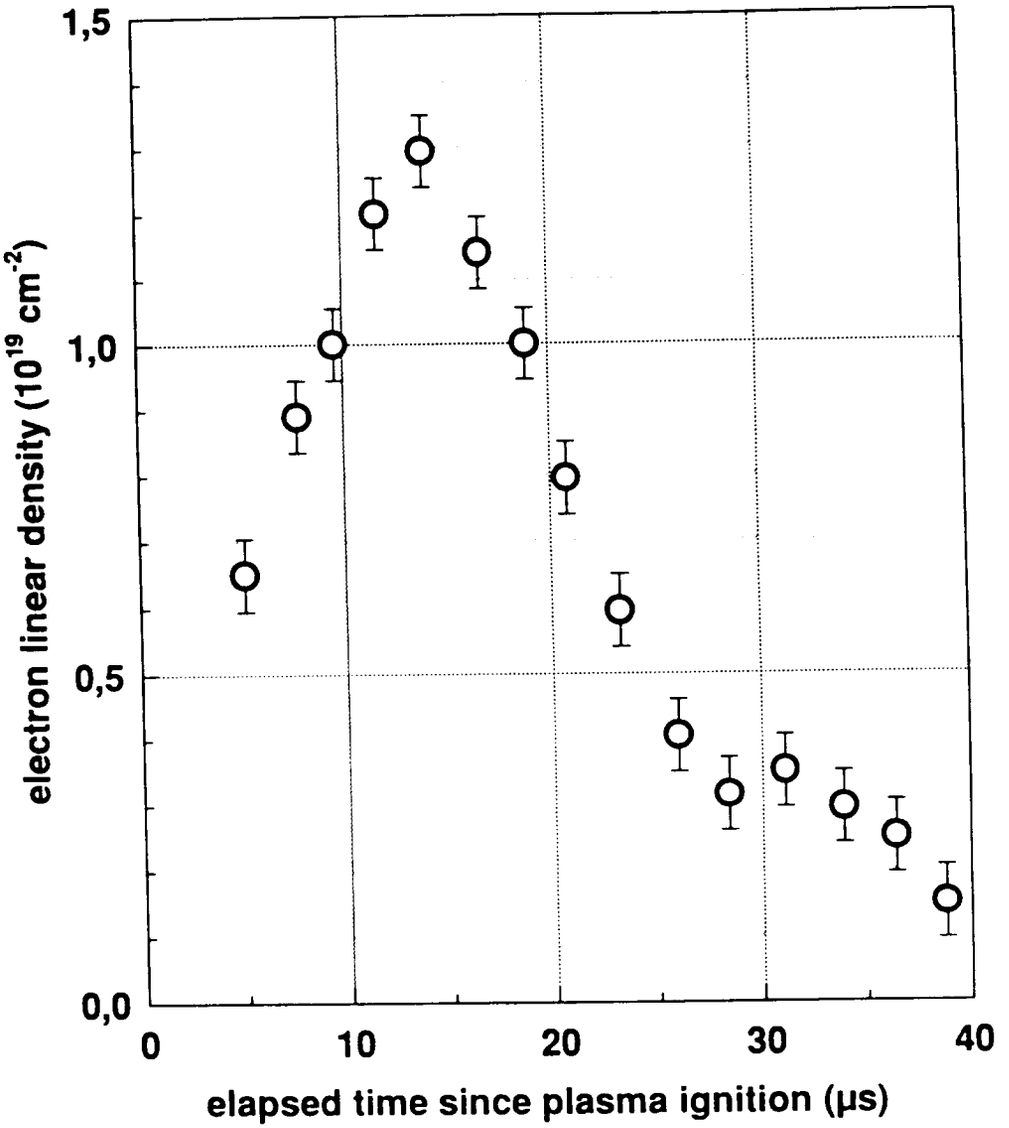

Figure 1: Plasma density as a function of time.

2-3 Magnetic spectrometer and detection system

After interaction with the target, the beam was magnetically analyzed. A slit in front of a magnetic spectrometer defined the entrance trajectories. The position of the ion impact after deflection by the magnetic field, was detected by a plastic scintillator (NE102A, 1mm thick), viewed by a fast camera which produced intensified images on a charge coupled device (CCD). The CCD output was connected to a digital computer interface.

2-4 Data analysis

The background of the CCD noise was subtracted for each image. Afterwards, the images were projected along the dispersive direction. The resulting charge distributions were fitted by convolution of Gaussian distributions using the PAW software library from CERN [11]. The area under each peak profile was proportional to the number of detected ions of a specific charge state. An example of a charge-state distribution is given in Fig.(2).

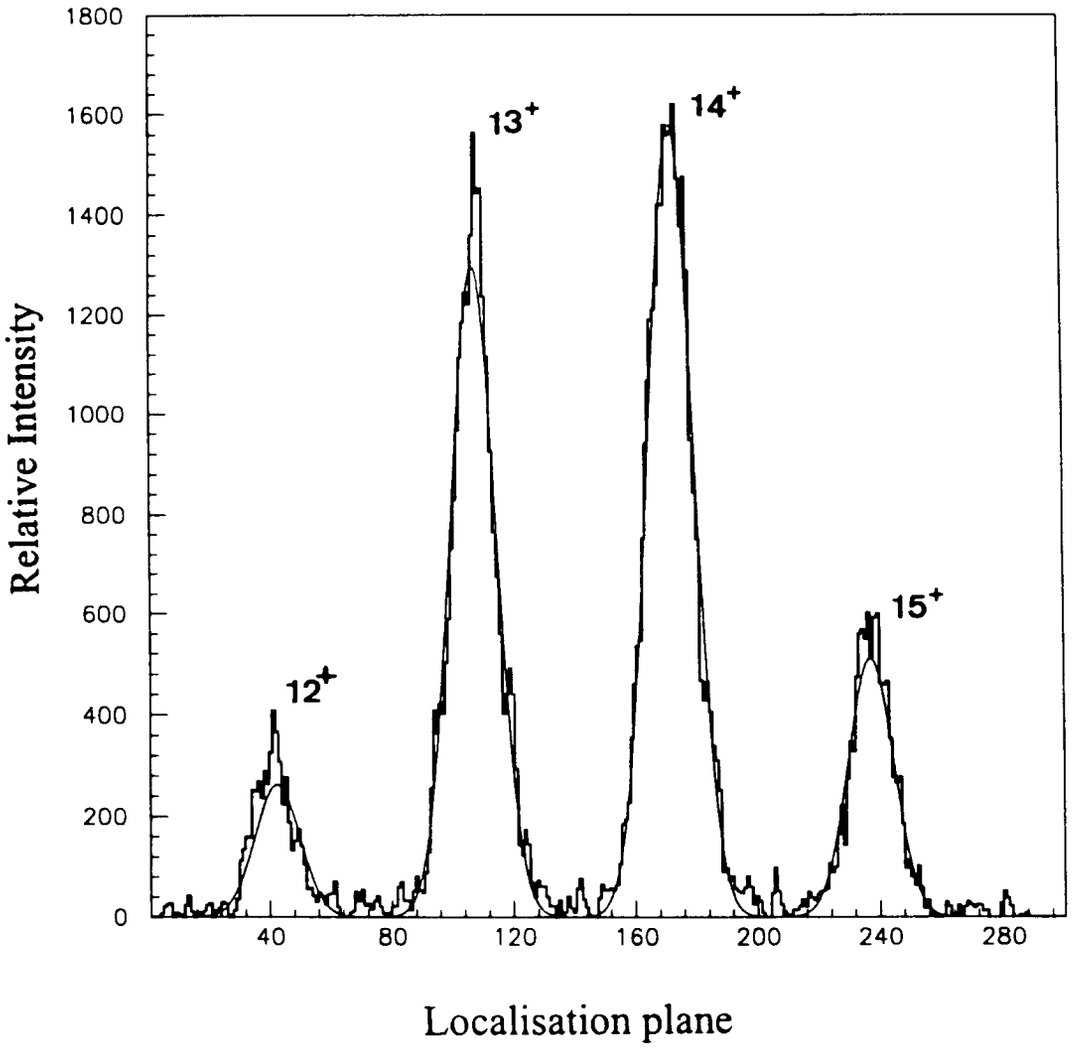

Figure 2: Charge state distribution for Cl ions obtained on the plastic scintillator. The histogram corresponds to the data and the solid line to the gaussian fit.

2-5 Perturbation due to plasma lens effects

A specific feature of the linear discharge comes from the generation of an intense azimuthal magnetic field varying linearly from zero value on the axis to a maximum value on the outer radius r:

$$B = \mu_0 jr / 2$$

where j is the current density and r the radius of the column. The beam interacting with the plasma column is collinear with the current direction.(Fig 3). Depending on the relative directions of the current and of the beam, the Lorentz force has a strong radial component and tends to focus or defocus the ion beam. Such a property of the linear plasma discharge has been extensively studied to generate efficient plasma lenses [12-13]. In the case of charge-state measurements, this effect is a real nuisance because for a given value of the current, the focal length F is a function of the beam charge-state:

$$F = \left(\sqrt{k} \times \sin(\sqrt{k} \times l)\right)^{-1}$$

with: $$k = \frac{q}{p} \times \mu_0 \times \frac{j}{2}$$

Where l is the plasma length, p the ion momentum, and q the charge state of the ion.

As a consequence, the beam size at the entrance slits of the magnetic spectrometer depends on the charge state. The Fig.(3) illustrates this dependence on the transmitted intensity through the magnet slit.

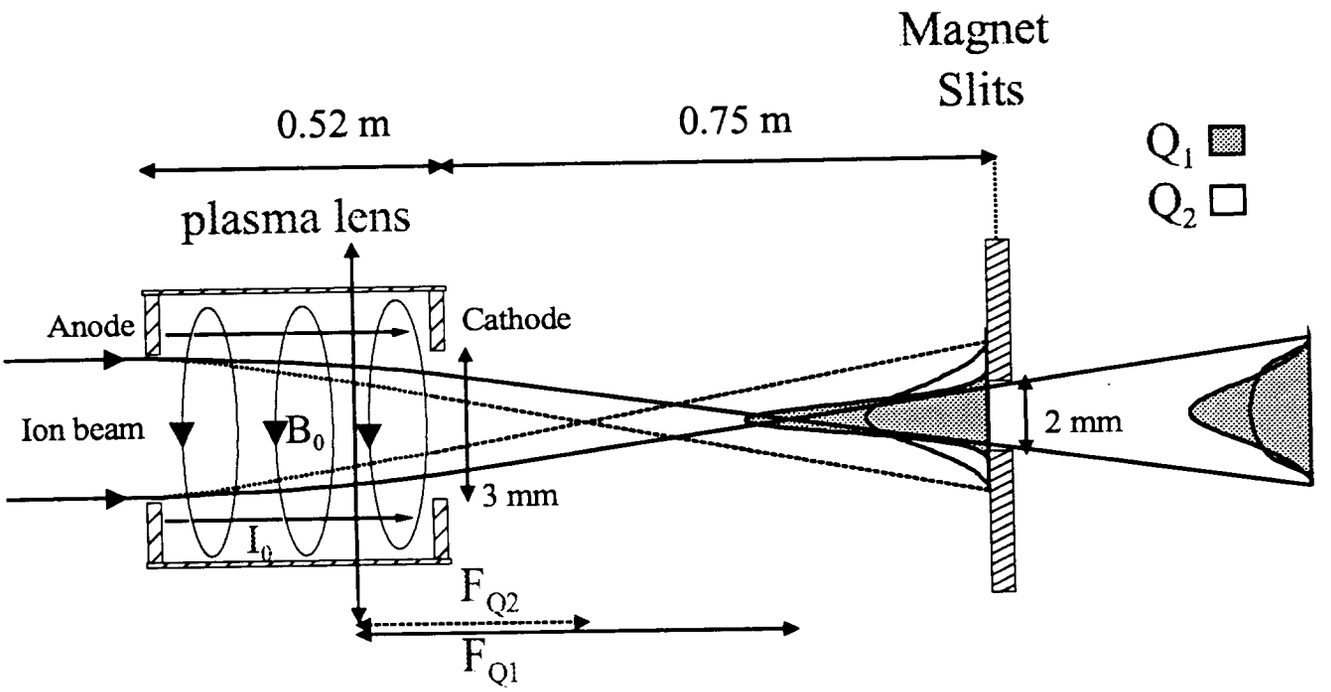

Figure 3: Plasma lens effect and its influence on the charge state distribution. The relative intensity passing through the slit depends on the focusing distance i.e. to the charge state of the ion.

To evaluate quantitatively this effect, a Monte-Carlo code was developed in which the initial velocity of individual ions was confined in a realistic phase-space emittance figure. A correction factor was deduced for the transmission through the slit of the different charge states. In the worst case this factor reached 50 % in relative abundance of the observed charge states.

In any case, a treatment of this plasma lens distortion must include the "charge history" during the travel through the plasma. This evolution is a key issue in the study. In order to overcome this problem, the results reported here are limited to the events which correspond to measurements independent on this effect, that is to say when the beam was strongly defocused for all charge states arriving on the slits. In this particular case, the transmission ratio defined by the slit aperture is the same for all the components of the charge state distribution.

3- Results and discussion

3-1 Cold gas measurements

3-1-1 Experimental charge state distributions

The evolution of the charge-state distributions as a function of the gas pressure was measured for two incident charge states of the projectile: 13^+ and 15^+ and a beam energy of 1.5 MeV/u. Experimental results are presented on Fig (4) and (5). Entering with a 13+ or 15+ chlorine ion leads to an equilibrium charge state equal to 13.18 ± 0.02. These values are in agreement with previous equilibrium charge state determination in hydrogen from [14]. Solid curves correspond to the model calculation presented in the next section.

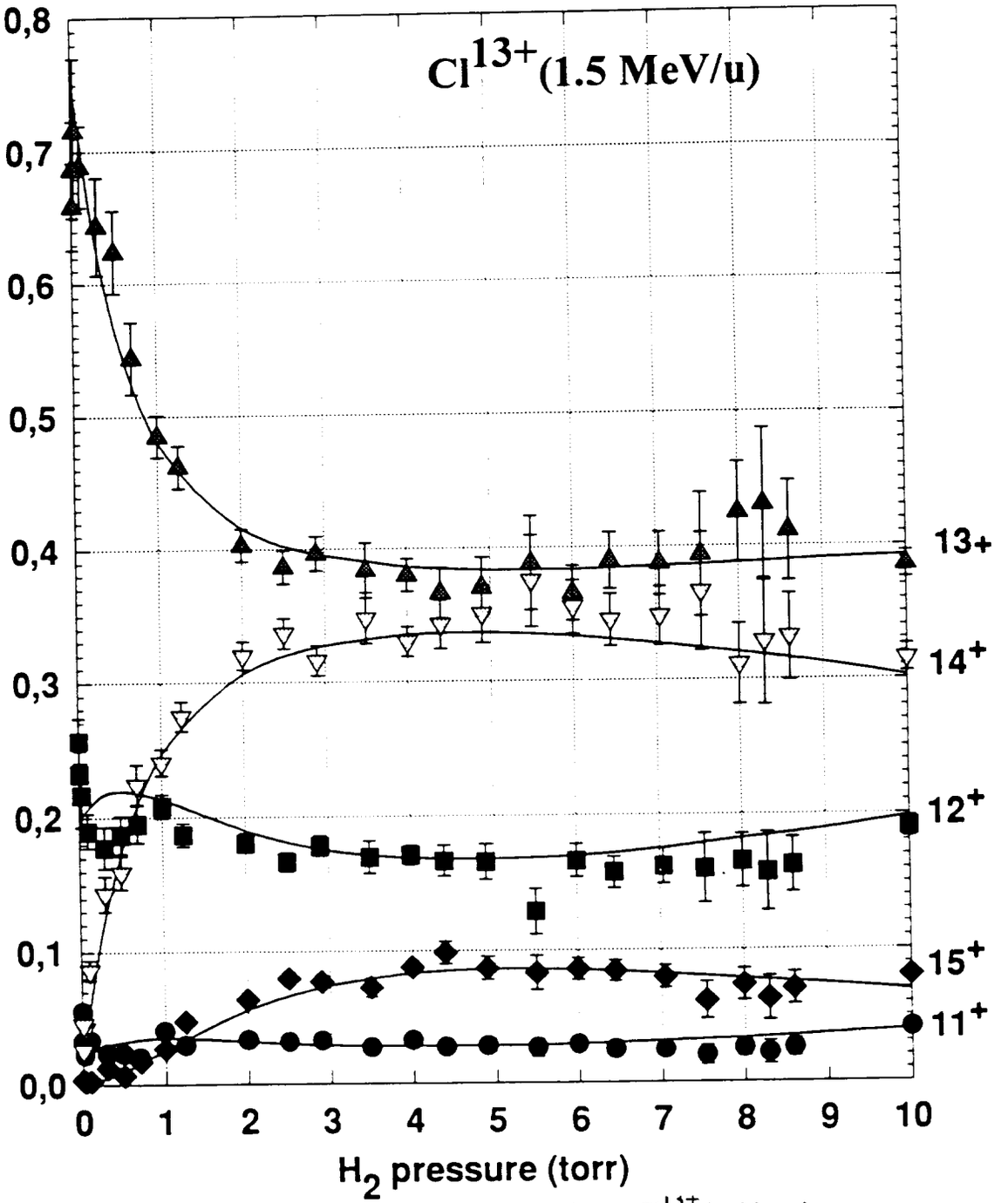

Figure 4: Charge state evolution in cold gas. Cl^{13+} incident ion.

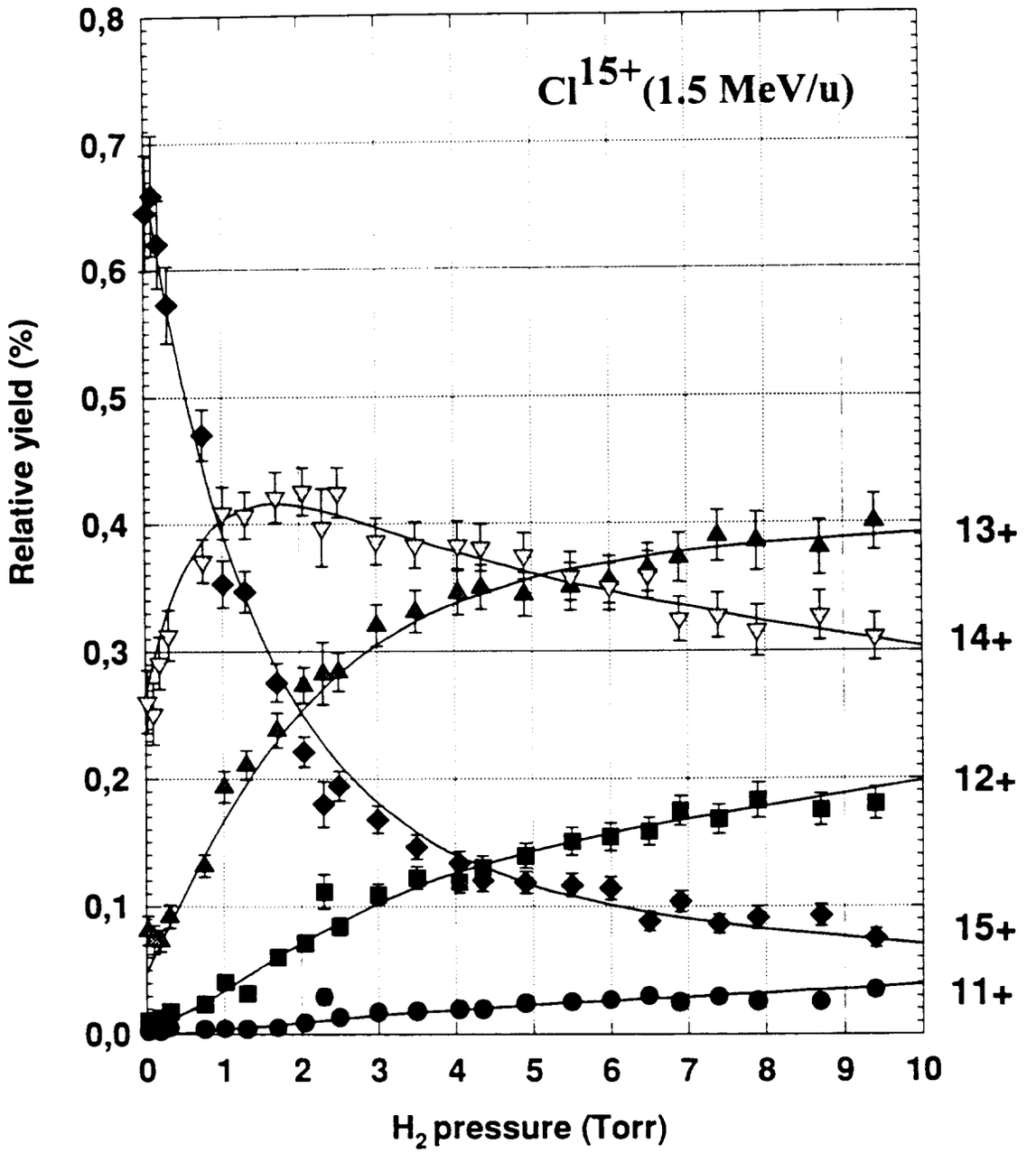

Figure 4: Charge state evolution in cold gas. Cl^{15+} incident ion.

3-1-2 Model calculation for cold gas

The final charge distributions of chlorine ions traversing various target thicknesses are obtained by solving the complete set of linear differential coupled equations governing capture and ionization rates. Double charge-exchange processes have been neglected and each of theserate equations couples a given charge state q to the two closest neighbor charge-state $q+1$ and $q-1$. The low density of the target (some 10^{17} H/cm^3) allows to consider that the ions, excited after each collision, do have enough time to return to their ground state before the next interaction. Metastable states have also been neglected. Therefore, cross-sections which are inserted in this calculation refer to ground-state configurations. Contributions from heavy impurities are also included in the model.

The cross sections for heavy impurities are deduced from measurements in residual gas, while the cross sections for hydrogen gas are adjusted to fit the experimental evolution of the charge state distribution with the target density for both incident Cl^{13+} (Fig.(4)), and Cl^{15+} (Fig.(5)) ion beams. The strong velocity dependence of capture cross-sections associated with the deceleration process of the chlorine ions during their travel through the gas cell has been well taken into account. The results of this calculation presented in Fig.(6) together with the constant velocity approximation, show that the velocity effect must be considered at high pressure measurements.

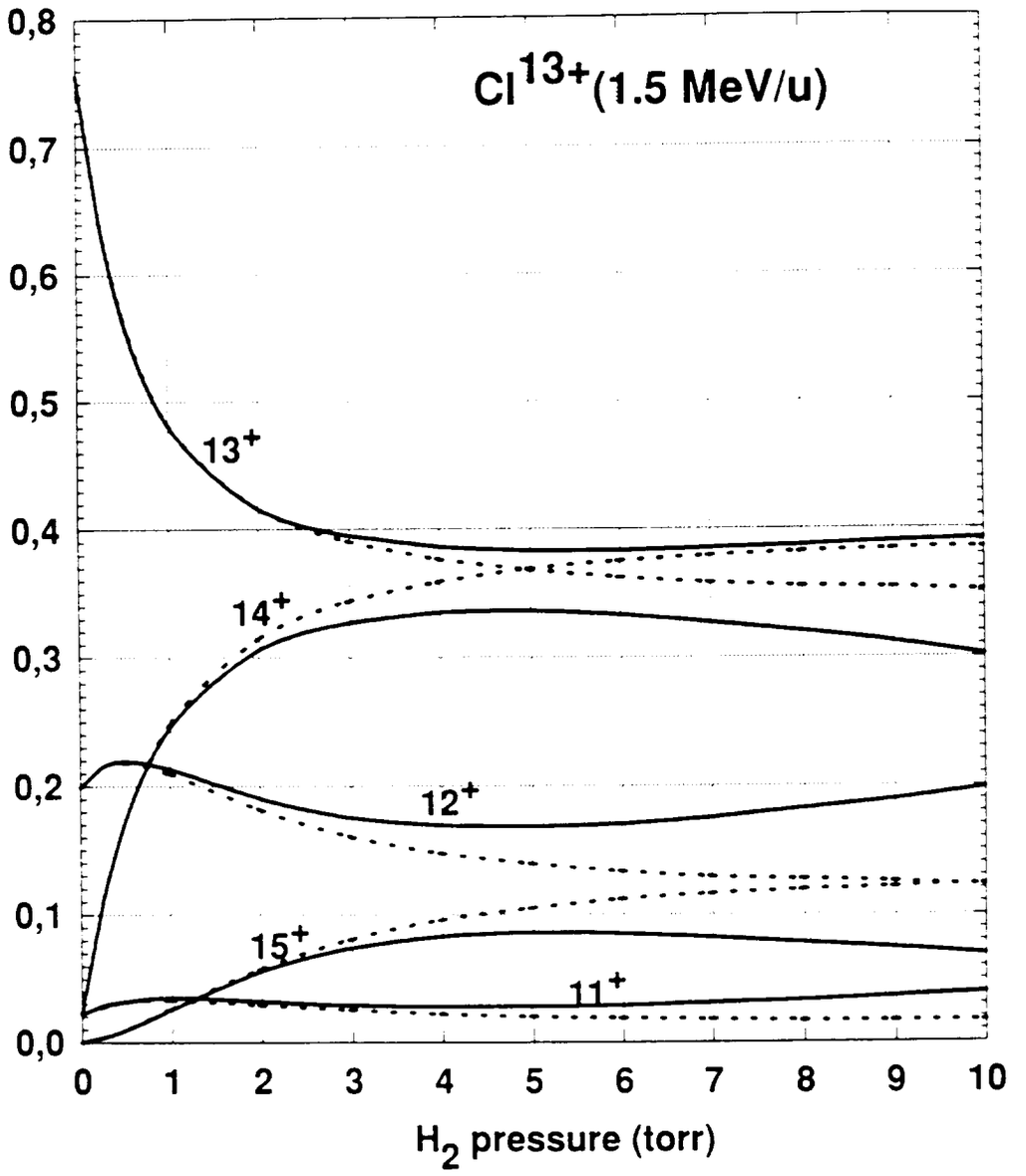

Figure 6: Velocity dependence on cold gas charge state distributions. Dotted curves correspond to the constant velocity approximation

3-1-3 Comparison with experimental results

Capture and ionization cross sections corresponding to the best fit of the cold gas charge state distributions are presented in tables (1) and (2) together with theoretical calculations and empirical predictions from ref. [19-25].
The Plane Wave Born Approximation (PWBA) has been applied to the proton ionization cross section [19,20]. Dependence on the projectile configuration uses effective charge deduced from ref. [21]. The value of the proton ionization cross-section (corrected PWBA) has been improved by introducing several corrections established by Brandt [22] who takes into account the Coulomb-deflection of the ion trajectory and a molecular effect in the vicinity of the hydrogen target atom at low velocities. At higher velocities a polarization term which corresponds to the second order term in the Born approximation is added to the theory. Screening effects due to the hydrogen electrons have been computed with a Thomas-Fermi approximation and found to be negligible. Ionization cross sections by free electrons are calculated by using the D.L.Moores formalism [23] and bound-electron ionization is estimated in the sudden impulse approximation. In this later case, the electron ionization cross-section is integrated over the full hydrogen momentum distribution.

Table 1 presents the total ionization cross sections associated with each charge state. The computed cross sections are compared with total ionization cross sections used in the code (last column). The values result from the contribution of all the electronic shell components to the ionization process. The agreement is remarkable and always stays within a 30% discrepancy. Capture cross-sections resulting from the fit are compared to Schlachter [24] and Nakaï [25] predictions in table 2 and found to lie within the confidence range given by these authors.

Table 1: Ionization cross-sections

Values are in (cm^2)

ION	last e^- config	PWBA proton	corrected PWBA	free electron	bound electron	sum proton + electron	sum used in code	total for all electrons	total used in code
Cl^{16+}	1s	7.53×10^{-22}	5.44×10^{-22}	0	2.54×10^{-27}	5.44×10^{-22}	1.07×10^{-21}	5.44×10^{-22}	1.07×10^{-21}*
Cl^{15+}	$1s^2$	9.85×10^{-22}	7.29×10^{-22}	0	4.00×10^{-27}	7.29×10^{-22}	1.34×10^{-21}	1.46×10^{-21}	2.67×10^{-21}*
Cl^{14+}	$1s^2$	1.08×10^{-21}	8.10×10^{-22}	0	4.74×10^{-27}	8.10×10^{-22}	1.34×10^{-21}		
Cl^{14+}	2s	6.67×10^{-20}	6.26×10^{-20}	6.77×10^{-22}	3.86×10^{-21}	6.49×10^{-20}	5.04×10^{-20}	6.65×10^{-20}	5.31×10^{-20}
Cl^{13+}	$1s^2$	1.18×10^{-21}	8.89×10^{-22}	0	5.54×10^{-27}	8.89×10^{-22}	1.34×10^{-21}		
Cl^{13+}	$2s^2$	7.59×10^{-20}	7.15×10^{-20}	7.02×10^{-21}	7.90×10^{-21}	7.90×10^{-20}	7.38×10^{-20}	1.60×10^{-19}	1.50×10^{-19}
Cl^{12+}	$1s^2$	1.32×10^{-21}	1.01×10^{-21}	0	6.87×10^{-27}	1.01×10^{-21}	1.34×10^{-21}		
Cl^{12+}	$2s^2$	8.61×10^{-20}	8.14×10^{-20}	1.40×10^{-20}	1.36×10^{-20}	9.52×10^{-20}	7.38×10^{-20}		
Cl^{12+}	2p	9.69×10^{-20}	9.51×10^{-20}	2.47×10^{-20}	2.35×10^{-20}	1.19×10^{-19}	1.67×10^{-19}	3.11×10^{-19}	3.17×10^{-19}
Cl^{11+}	$1s^2$	1.45×10^{-21}	1.13×10^{-21}	0	8.31×10^{-27}	1.13×10^{-21}	1.34×10^{-21}		
Cl^{11+}	$2s^2$	1.01×10^{-19}	9.56×10^{-20}	2.39×10^{-20}	2.29×10^{-20}	1.19×10^{-19}	7.38×10^{-20}		
Cl^{11+}	$2p^2$	1.16×10^{-19}	1.14×10^{-19}	3.89×10^{-20}	3.71×10^{-20}	1.52×10^{-19}	2.59×10^{-19}	5.44×10^{-19}	6.69×10^{-19}
Cl^{10+}	$1s^2$	1.61×10^{-21}	1.27×10^{-21}	0	1.03×10^{-26}	1.27×10^{-21}	1.34×10^{-21}		
Cl^{10+}	$2s^2$	1.17×10^{-19}	1.12×10^{-19}	3.50×10^{-20}	3.38×10^{-20}	1.46×10^{-19}	7.38×10^{-20}		
Cl^{10+}	$2p^3$	1.40×10^{-19}	1.38×10^{-19}	5.65×10^{-20}	5.45×10^{-20}	1.94×10^{-19}	2.79×10^{-19}	8.77×10^{-19}	9.84×10^{-19}*

* This cross section plays a minor role in the charge-state distribution.

Table 2: Capture cross-sections

Values are in (cm^2)

ION	Slachter	Nakaï	model values
Cl 17	3.51×10^{-19}	3.24×10^{-19}	2.43×10^{-19}*
Cl 16	2.78×10^{-19}	2.72×10^{-19}	2.07×10^{-19}*
Cl 15	2.17×10^{-19}	2.27×10^{-19}	1.70×10^{-19}
Cl 14	1.66×10^{-19}	1.86×10^{-19}	1.40×10^{-19}
Cl 13	1.25×10^{-19}	1.51×10^{-19}	1.13×10^{-19}
Cl 12	9.16×10^{-20}	1.20×10^{-19}	9.00×10^{-20}
Cl 11	6.54×10^{-20}	9.36×10^{-20}	4.02×10^{-20}*
Cl 10	4.53×10^{-20}	7.13×10^{-20}	3.96×10^{-20}*

*This cross section plays a minor role in the charge-state distribution.

3-2 Plasma measurements

3-2-1 Experimental results

For the two incident charge states 13^+ and 15^+, the final charge-state distributions after interaction with fully ionized hydrogen, are compared in Fig (7) and (8) with the corresponding cold gas distributions. This comparison has been performed during the optimum transmission period (see § 2-5). At this moment the linear density of the target was $1.10^{19} \pm 0.1$ e^-/cm^2. The enhancement of the stripping efficiency of the plasma medium appears clearly with the 13^+ incident projectile. The mean charge state is displaced from 13.18 up to 13.87 in the plasma case. For the 15^+ incident charge Fig (8), a frozen charge-state effect is observed, in analogy with channeling experiments [15,16]. The error bars which are reported on the graphs reflect experimental uncertainties on peak localization, Gaussian fitting, and remaining plasma lens effects.

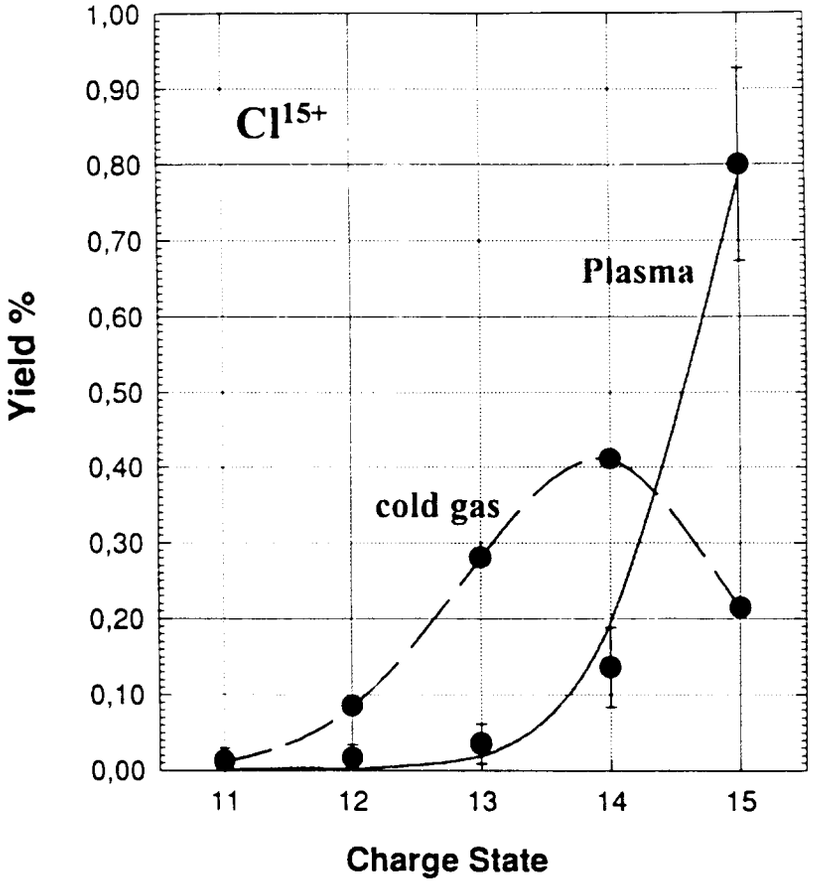

Figure 7: Comparison between cold gas and plasma charge state distribution. Cl^{13+} incident ion. The lines represent the model calculation for cold gas (dashed line) or plasma (solid line).

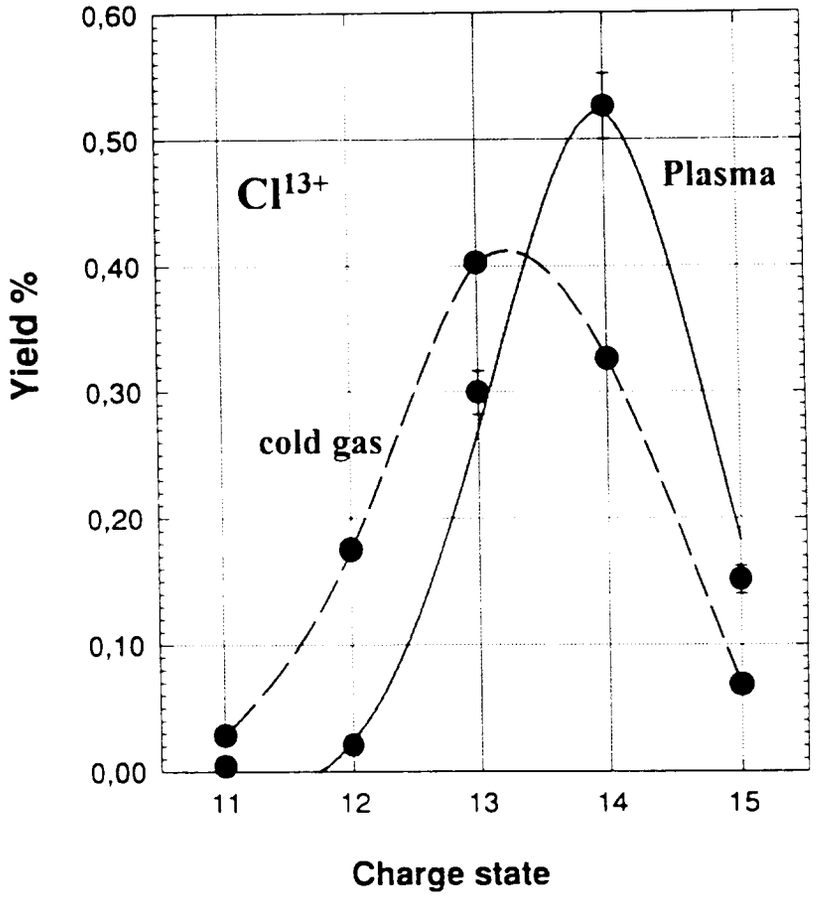

Figure 8: Comparison between cold gas and plasma charge state distribution. Cl^{15+} incident ion.

3-2-2 Plasma calculation

The calculation in the plasma case is based on the following three assumptions:

-i) The capture cross section of free electrons is zero.

This approximation is justified considering that the cross sections associated to radiative charge transfer are roughly three order of magnitude lower than the bound electron capture cross sections. Moreover, dielectronic recombination processes are determined by resonant features which need not to be considered in this particular velocity range [17]

-ii) The ionization cross section for the free electron-proton pair is taken to be half the ionization cross section for the hydrogen molecule. That is to say that proton is not screened by bound electron and that ionization by bound or free electrons is equal.

-iii) The cross sections on the impurities are the same in the cold gas and in the plasma medium.

The plasma temperature (2 eV) is not high enough to ionize more than one outer shell electron on heavy impurities. This electron gives only a small contribution on the total charge transfer cross section [18] and its role on the screening remains negligible for the ionization process.

3-2-3 Comparison with the model

On Fig (4-5-7-8) are reported the calculated distributions (full curves) corresponding to the above assumptions. Within the experimental error bars, the agreement between experimental and computed charge state distributions is remarkable and comforts the validity of this simple modelisation. The theoretical cross sections presented in table 2 are well established, thus the agreement between cross sections used to fit the experimental data and the calculated values for both cold and hot target, tends to show that the basic physical issues corresponding to the plasma are included in such a phenomenological model.

3-3 Discussion

The influence of the plasma on the charge evolution is illustrated in fig. (9). Using the atomic cross sections of tables (1-2), we present the atomic rates for ionization τ_i and for capture of one electron τ_e in terms of the projectile charge state for both cold gas and plasma target:

$$\tau_i = (n_e \sigma_i^H + n_i \sigma_i^I) V$$

$$\tau_c = (n_H \sigma_c^H + n_i \sigma_c^I) V$$

where n_e, n_i and n_H are the electron (bound and free), impurity, and atomic hydrogen densities. $\sigma_{i,c}^H$ and $\sigma_{i,c}^I$ are the atomic cross sections for collisions with atomic hydrogen and impurities. V is the projectile velocity.

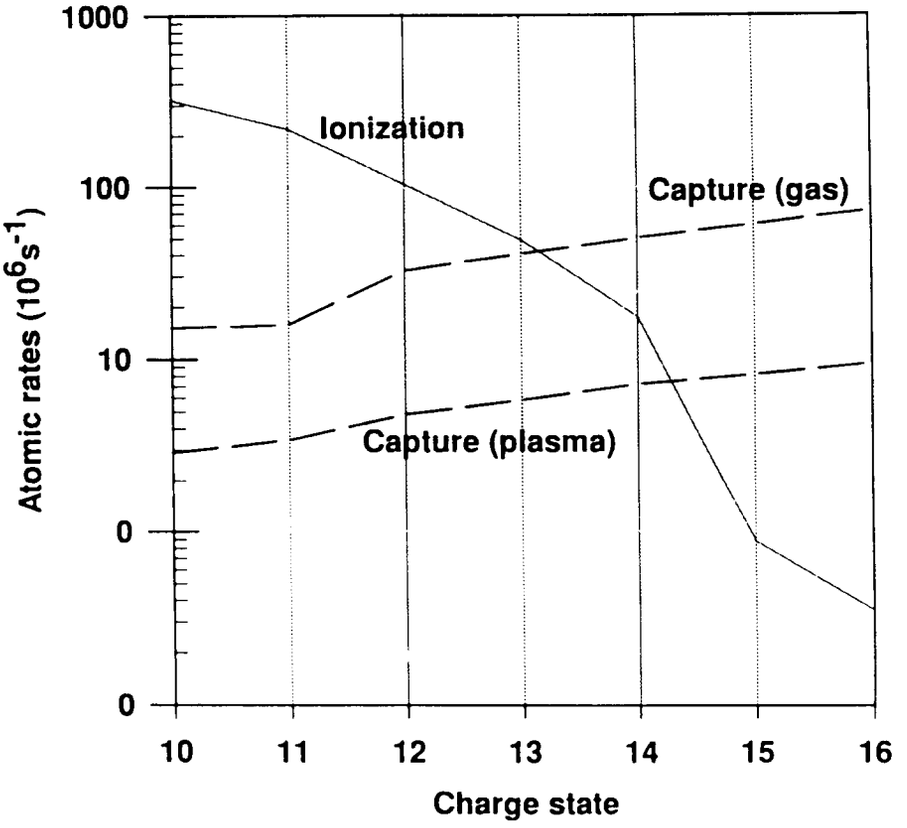

Figure 9: Ionization and one electron capture rates versus the projectile charge state for Cl^{q+} of 1.5 MeV/u in gas and plasma target.

The figure 9 clearly demonstrates the charge changing behaviour due to the plasma target: An unchanged ionization and a strongly reduced capture. In the plasma case the residual capture arises only from the remaining neutral hydrogen (some percent of the the total density) and also from the heavy impurities.
The crossing between the ionization and the capture curves correspond to the equilibrium charge values. In the gas case, we retrieve the experimental value of 13.2

In the general case of ion interaction with matter, three media can be distinguished for charge changing:

The cold gas medium where all the ionization and capture processes are effective.

The free electron medium, like in channeling experiments, where the main capture and ionization processes are suppressed (no more ionization by nuclei).

The plasma medium where capture is reduced, like in channeling experiments, but where ionization on nuclei remains valid.

The consequence is that plasma is the most effective stripping medium for heavy ions beams in the MeV/u velocity range.

4-Conclusion

This paper presents a clear experimental evidence for the plasma stripping enhancement. For the chlorine ions which are considered in this article, the difference between cold gas and plasma increases with a decreasing beam velocity. At 2 MeV/u and with a plasma density of 1.10^{19} cm^{-2}, this effect remains negligible [9]. At 1.5 MeV/u and at the same plasma density, the charge state distribution of Cl^{13+} incident ions is shifted toward higher values than in the corresponding cold gas medium. This velocity dependence, but also the complexity of the plasma apparatus and the timing constraint limits the ability of such a process in accelerator applications. On the other hand, this behavior is of great interest for the study of inertial confinement fusion driven by heavy ions, because the stopping process is largely determined by the dynamically controlled evolution of the charge state of the projectile.

Further experiments are necessary to investigate more accurately the correlation between the projectile charge state evolution and the corresponding stopping power amplitude and straggling in the plasma target.

References

1- G.D.Alton, R.A.Sparrow and R.E. Olson
Phys.Rev.A Vol 45,Nb 8 (1992) 5957

2- E.Nardi, Z.Zinamon
Phys.Rev.Lett. 49 (1982) 1251

3- D.H.H.Hoffmann, K.Weyrich, H.Wahl, D.Gardès, R.Bimbot and C.Fleurier.
Phys.Rev. A Vol 42,4 (1990) 2313

4- D.Gardès, A.Servajean, B.Kubica, C.Fleurier, D.Hong, C.Deutsch and G.Maynard.
Phys.Rev. A Vol 46,8 (1992) 5101

5- G.Maynard, W.André, M.Chabot, C.Deutsch, C.Fleurier, D.Gardès, D.Hong, J.Kiener, M.Pouey and K.Wohrer.
Il Nuovo Cimento 106,12 (1994) 1825

6- T.Peter and J.Meyer-ter-Vehn
Phys.Rev.A 43,4 (1991) 2015

7- C.Fleurier, J.Mathias, B.Dumax, J.Pellicer, A.Bonnet, D.Gardès and B.Kubica.
Nucl.Instr. and Methods B 61 (1991) 236

8- C.Fleurier, A.Sanba, D.Hong, J.Mathias and J.C.Pellicer
Journal de Physique C7, 49 (1988) 141

9- M.Chabot, D.Gardès, J.Kiener, S.Damache, B.Kubica, C.Deutsch, G.Maynard, M.Pouey, W.André, C.Fleurier, D.Hong and K.Wohrer.
Il Nuovo Cimento 106 A,12 (1993) 1789

10- M.Chabot et al
Laser and Particle Beams. To be published

11- Physics Analysis Workstation (PAW)
Computing and Networks Division - CERN, Geneva

12- E.Boggasch, J.Jacoby, H.Wahl, K.G.Dietrich, D.H.H.Hoffmann, W.Laux, M.Elfers, C.R.Haas, V.P.Dubenkov and A.A.Golubev
Phys.Rev.Lett. 66,13 (1991) 1705

13- A.Tauschwitz, E.Boggasch, D.H.H.Hoffmann, M.de Magistris, U.Neuner, M.Stetter, R.Tkotz, T.Wagner, W.Seelig and H.Wetzler
Il Nuovo Cimento 106 A,12 (1993) 1733

14- R.Bimbot and M.F.Rivet, to be published

15- J.A.Golovchenko, A.N.Goland, J.S.Rosner, C.E.Thorn, H.E.Wegner, H.Knudsen and C.D.Moak
Phys.Rev. B Vol 23,3 (1981) 957

16- S.Andriamonje, B.Blank, R.del Moral, J.P.Dufour, L.Faux, A.Fleury, M.S.Pravikoff, C.Röhl, M.Chevallier, D.Dauvergne, R.Kirsh, J.C.Poisat, J.Remilleux, C.Cohen, Y.Girard, A.L'Hoir, J.P.Rozet, D.Schmaus, D.Vernhet, J.Dural, H.Rothard, M.Toulemonde, Y.Quéré and N.Cue
Nucl. Instr. and Methods in Phys.Res. B 87 (1994) 116

17- G.Maynard and C.Deutsch
Phys. Scripta Vol 48 (1993) 471

18- D. Z. Belkic, R. Gayet and A. Salin
Phys. Rep. Vol 6 (1979) 279

19- G.S.Khandelwal, B.H.Choi and E.Merzbacher
Atom.Data vol 1 (1969) 103

20- B.H.Choi, E.Merzbacher and G.S.Khandelwal
Atom.Data Vol 5 (1973) 291

21- R.Marchand, S.Caillée and Y.T.Lee
J.of Quant.Spectr.Radiat.Transfer Vol 43 (1990) 149

22- W.Brandt and G.Lapicki
Phys.Rev.A 20 (1979) 465

23- D.L.Moores, L.B.Golden and D.H.Sampson
J.Phys.B: Atom.Molec.Phys. 13 (1980) 385

24- A.S. Schlachter, J.W.Stearns, W.G.Graham, K.A.Berkner, R.V.Pyle and J.A.Tanis
Phys.Rev.A 27 (1983) 3372

25- Y.Nakaï, M.Shirai, T.Tabata and R.Ito
At.Data and Nucl. Data Table 37 (1987) 69

26- N.Bohr and J.Lindhard
Kgl.Danske Videnskab Selskab, Mat.Fys.Medd. 28,7 (1954)

27- H.D.Betz and L.Grodzins
Phys.Rev.Lett. 25,4 (1970) 211